Correlation between the edge and the internal transport barriers in JT-60U

Y. Kamada, M. Yoshida, Y. Sakamoto, Y. Koide, N. Oyama, H. Urano, K. Kamiya
T. Suzuki, A. Isayama, and the JT-60 Team

Japan Atomic Energy Agency, Naka, Ibaraki-ken, 311-0193 Japan

e-mail contact of main author : kamada.yutaka@jaea.go.jp

Abstract. For understanding of the physics processes determining the radial profiles of the plasma pressure in the advanced tokamak plasmas, correlation between the edge and the internal transport barriers (ETB and ITB) has been studied. We fond that the edge pedestal beta, $\beta_{p\text{-}ped}$, increases almost linearly with the total β_p over a wide range of the plasma current for the type I ELMing H-mode, and the dependence becomes stronger with increasing triangularity. This dependence is not due to the profile stiffness. However, with increasing the stored energy inside ITB (W_{ITB}), the total thermal stored energy (W_{th}) increases and then the pedestal stored energy (W_{ped}) increases. With increasing W_{ped}, the ELM penetration depth expands more inward and finally reaches the ITB-foot radius. At this situation, the ITB radius cannot move outward and the ITB strength becomes weak. Then the fractions of W_{ITB} and W_{ped} to W_{th} become almost constant. We also found that the type I ELM expels/decreases edge toroidal momentum larger than ion thermal energy. The ELM penetration radius for toroidal rotation tends to be deeper than that for ion temperature, and can exceeds the ITB radius. The ELM affected area is deeper for CO rotating plasmas than CTR rotating ones. The ELM affected area is deeper in the order of the toroidal rotation (V_t), the ion temperature (T_i) and then the electron temperature (T_e). The L-H transition also changes the V_t-profile more significantly than the T_i-profile. After the L-H transition, in the ELM-free phase, the pedestal Vt sifts into the CTR direction deeply and suddenly, and after that the pedestal V_t and T_i evolves in the similar timescale. The change in V_t by ELM and L-H transition may affect degradation / evolution of ITBs.

1. Introduction

In order to sustain burning plasmas in ITER and power plants, we need to achieve high values of energy confinement time, normalized beta, bootstrap current fraction simultaneously. Towards this goal, the world tokamaks have been developing the advanced operation modes characterized by the edge transport barrier (ETB) and the internal transport barrier (ITB). Since radial shapes of the kinetic parameters play the central roles for all of the above performances, it is critical to understand the physics processes determining the radial profiles. For both ETB and ITB, their radial structure and evolution have been studied significantly [1,2]. However, the correlation between these two transport barriers remains still as an open issue. The correlation, if it exists, determines the whole radial profiles and then determines the dynamics of the advanced tokamak plasma system. In order to address this issue, correlation between the edge transport barrier and the internal transport barrier has been studied in JT-60U for Type I ELMing plasmas. This paper is arranges as follows: Section 2 treats the pedestal plasma pressure enhanced with core pressure. Section 3 deals with dependence of the stored energy sustained by ETB and ITB, and their relationship. Section 4 treats relationship of ITB radius and ELM penetration. Section 5 and 6 treat change in rotation and temperature profiles by ELMs and L-H transition, respectively. Section 7 gives summary.

2. Pedestal pressure enhanced with core pressure

JT-60U revealed that the pedestal β_p and the normalized pressure gradient α for type I

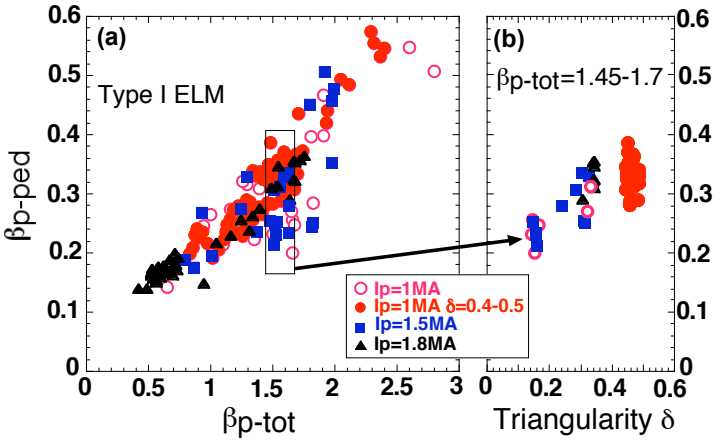

Fig.1 (a) Increasing βp-ped with βp-tot for I_p=1 - 1.8MA type I ELMing discharges, and (b) increasing βp-ped with trianglarity at fixed βp-tot (=1.45-1.7).

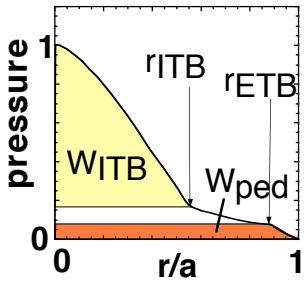

Fig.2 A schematic profile of the plasma pressure with ITB and an ET). Definition of W_{ITB} (the stored energy sustained by ITB) and W_{ped} (the stored energy sustained by ETB) , the ITB-foot radius (r_{ITB}) and the pedestal-top radius (r_{ETB}) are given.

ELMing H-mode increase with increasing total β_p (β_p-tot) when triangularity δ is high [3,4], and the world tokamak data supported this dependence [5]. Based on this knowledge, we have expanded the understanding of the pedestal stored energy evolving with the core energy. Figure 1 shows the dependence of β_p-ped on β_p-tot for the positive magnetic shear discharges including both the standard H-mode and the high β_p H-mode with ITB at different plasma current I_p and δ. As shown in Fig.1(a), β_p-ped increases with β_p-tot in this wide range of plasma parameters. In particular clear linearly can be concluded at I_p=1MA and δ=0.4-0.5 (closed circles). This dependence is not due to the profile stiffness because the dependence is the same for discharges both with and without ITB (see Fig.2(c)). Figure 1(b) treats the data at the fixed β_p-tot=1.45-1.7 enclosed by the square in Fig.1(a). The β_p-ped values increase with trianglarity. This dependences is almost the same over a wide range of I_p = 1- 1.8MA, and q_{95}=3.2 - 6.2.

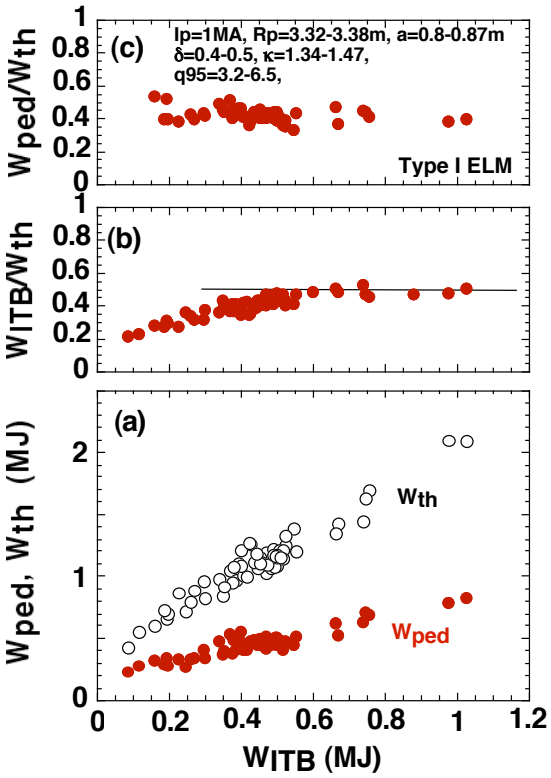

Fig.3: Dependence of (a) W_{ped}, W_{th}, (b) W_{ITB}/W_{th} and (c) W_{ped}/W_{th} on W_{ITB} for type-I ELMing discharges at I_p=1MA, δ=0.4-0.5.

3. Dependence of W_{PED}/W_{th} and W_{ITB}/W_{th}

In the previous section, we confirmed that the total stored energy (βp-tot) determines the pedestal stored energy (βp-ped). Next question is how the total stored energy depends upon the ITB. In high β_p H-mode, the total thermal stored energy (W_{th}) increases with increasing stored energy sustained by ITB (W_{ITB}; defined in the pressure profile in Fig 2). Figure 3 treats the data at fixed I_p=1MA (δ=0.4-0.5). The

increase in W_{ITB} is due to expansion of the ITB-foot radius and/or increasing pressure gradient inside ITB. As shown in Fig.3(b), W_{ITB}/W_{th} increases with increasing W_{ITB}, then saturate around W_{ITB}/W_{th} ~0.5. On the other hand, W_{ped}/W_{th} is almost constant around ~0.4 (as expected from Fig.1), where W_{ped} is the stored energy sustained by ETB (see Fig.2 again). This means that the contribution of ITB to the total stored energy is increasing at first, then the fraction of W_{ped} and W_{ITB} to W_{th} becomes constant (a kind of profile stiffness with ITB and ETB). This saturation seems to be due to the effects of ELMs as shown below.

4. ITB radius and ELM penetration

The ITB-foot radius seems to be affected by ELM penetration. Figure 4 shows time evolution of (a) the pedestal stored energy W_{ped} and the total stored energy W_{tot} and (b) the ELM penetration radius and the radial locations of ITB-foot and pedestal-top for a discharge at I_p=1.8MA. The pedestal energy W_{ped} increases with increasing W_{tot}, (W_{ped}/W_{tot} ~ const.), and the ELM penetration (evaluated by T_e measured by ECE) deepens with increasing W_{ped}. In the early phase (t<5.8s) the ITB-foot radius expands, and the radii of the pedestal top and the ELM penetration deepen gradually. Then the ELM penetration radius and the ITB foot meet to each other at t~5.8s. After that, the 'balanced phase' lasts for ~0.7s. Interestingly, the ITB foot seems to behave as a barrier against the ELM penetration (t= 5.8 - 5.95s and 6.25 - 6.49s), and after around ten ELM attacks the ITB foot shrinks (t=5.95 - 6.0s and t=6.49 - 6.55s). Then the ELM penetration follows the shrinking ITB-foot. Thus, the ELM crash affects the ITB radius.

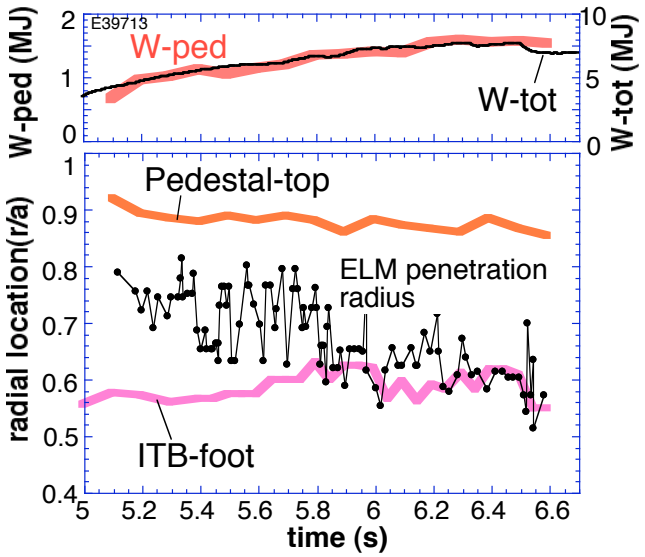

Fig.4: Evolution of Wped, W-tot, ELM penetration radius, pedestal-top radius, ITB-foot radius for a type-I ELMing high β_p H-mode discharge (I_p=1.8MA, Bt=4.05T, δ=0.34, κ=1.51, q_{95}=4.1, P_{inj}=22.4MW with 4.4MW of CO-tangential and 0.9MW of CTR-tangential NBs and 5.6MW of N-NB).

5. Change in rotation and temperature profiles by ELM

The above section 4 suggested the erosion by ELMs affects the ITB dynamics. Since, in the previous studies on ITB [6,7], the radial electric field shear plays a role for ITB formation, it is important to evaluate the change of toroidal rotation Vt and ion temperature Ti (pressure) by ELMs. Figure 5 (a) shows time evolution of T_i V_t from L-phase, ELMfree-H phase to ELMing-H phase for a discharge at I_p=2MA with balanced NB injection. The ITB is produced at first, then L-H transition occurs at t=5.8s, and T_i and V_t in the edge region increase rapidly. The counter (CTR) directed V_t is due to the ripple loss [8], intrinsic rotation by pressure gradient [9] and spontaneous spin-up at the H-mode edge (see Sec.6). The Type I ELM starts at t=6.1s, and T_i and V_t decreases suddenly. In the L and ELM-free phases, the ITB radius is

at r/a~0.75 (Fig,5(b)). Once ELM occurs, the rotation shear is lost at this radius, and ITB becomes weak. The change in the volume integral of ion thermal energy and momentum in the volume of 0.76 <r/a<1.0 (defined by (ELMing - L) / (ELMfree - L)) is 79% for ion thermal energy and 46% for momentum. This means that the loss of momentum by ELMs is much larger than that of the thermal energy. This large change in V_t profile may affects the ITB strength.

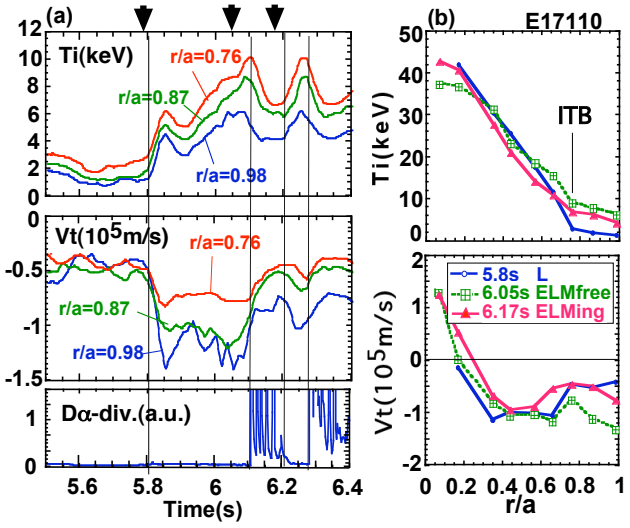

Fig.5: (a) Evolution of edge T_i and V_t and divertor D_α emission, and (b) profiles of T_i and V_t for L-, ELMfree and ELMing phases for a high β_p mode discharge (I_p=2MA, Bt=4.4T, δ=0.1, κ=1.80, q_{95}=3.67, P_{inj}=28.2MW with 4.4MW of CO-tangential and 4.7MW of CTR-tangential NBs).

In order to clarify the ELM effects on V_t and T_i with higher time resolution, Fig. 6 shows $T_i(r)$ and $V_t(r)$ before ELM crash, and $\Delta T_i/T_i$ and $\Delta V_t/V_t$ across ELM for a CO- and PERP-NB injected discahrge, where Δ means the difference between -2.5ms and + 5ms relative to the ELM crash. The ELM affected area for V_t is wider than that for T_i, and exceeds the ITB-foot radius, and $\Delta V_t/V_t > \Delta T_i/T_i$. This change in V_t at 0.5<r/a<0.8 does not seem to be due to loss of the intrinsic rotation [9], since the pressure gradient in this region stays almost constant. (Note: Evaluation of $\Delta V_t/V_t$ and comparison of $\Delta V_t/V_t$ to $\Delta T_i/T_i$ has meaning only when the Vt profile is well in the CO or CTR space without V_t=0 location, and the profile shape is similar to Ti(r) as in the case of Fig.6.)

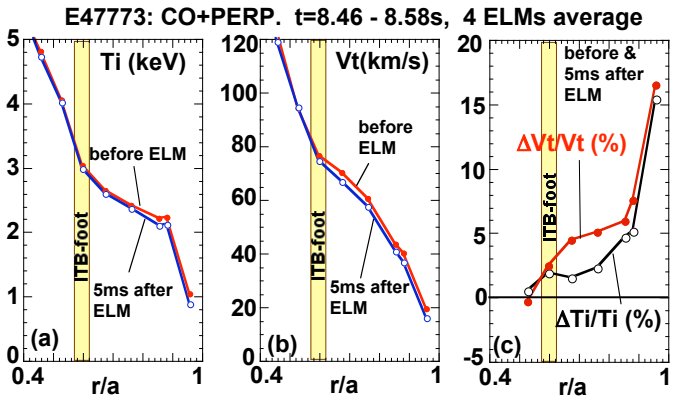

Fig.6: Profiles of (a) T_i, (b) V_t, and (c) change in T_i and V_t profiles across ELM crash (just before the type I ELM crash and 5ms after the crash averaged for 4 ELMs) for a Type I ELMing high βp H-mode discharge (I_p=0.85MA, Bt=2.4T, δ=0.38, κ=1.40, q_{95}=4.49, P_{inj}=9.5MW with 4.2MW of CO-tangential and 0.8MW of CTR-tangential NBs)

The erosion by the type-I ELM crash depends upon the size of the ELM. It is known that the ELM size depends on the toroidal rotation at the pedestal and CO-NB injection case has larger ELM than CTR-NB injection case [10,11]. In order to evaluate the dependence of erosion on the ELM size, Figs. 7 compares time evolution of CO-NB injection (Fig.7(a)) and CTR-NB injection (Fig.7(b)) across a few ELMs for standard H-mode discharges without ITB at I_p=1.6MA. (Except the NB injection direction, other operational parameters are the same for

these two discharges.) In case of CO-injection, the drop of the stored energy (W_{dia}) by the ELM is large ($\Delta W_{dia}/W_{dia}$~6%), the ELM period is long, change in V_t and T_i is clearly visible even in the core region (r/a~0.5). On the other hand, in case of CTR-injection, $\Delta W_{dia}/W_{dia}$ is small (~2%), the ELM period is short, change in V_t and T_i is small.

In addition, in case of CO-injection, the pedestal rotation (r/a=0.94) is counter directed, and V_t changes to V_t=0 (in other words, shift in the CO-direction) after the ELM crash. This shift in the CO-direction is discussed in the next section.

Figure 8 shows change in the V_t and T_i profiles across the ELM crash (again -2.5ms & +5ms relative to the ELM crash) and profiles of $\Delta V_t/V_t$, $\Delta T_i/T_i$, and $\Delta T_e/T_e$. ($\Delta T_e/T_e$ is evaluated -1ms and +2.5ms.) for the same discharges shown in Fig.7. Again the change in V_t and T_i profiles is large for CO-injection case than CTR-injection. The ELM affected area is deeper in the order of V_t (r), T_i(r) and then T_e in both CO and CTR cases.

Here, it should be noted that the T_i and V_t measurement by CXRS (time resolution = 2.5ms) has relatively worth S/N ratio just at the ELM crash due to background noise. So, we eliminated the data just at the ELM crash and +2.5ms in this evaluation. Therefore, the evaluation of $\Delta V_t/V_t$ and $\Delta T_i/T_i$ in this paper does not mean the ELM-eigenfunction distributiution itself from the view point of MHD

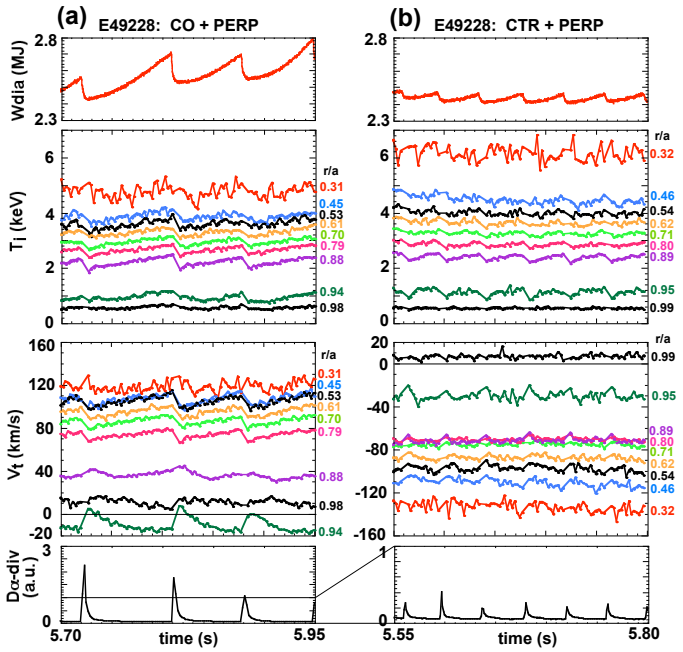

Fig.7: Comparison of 'Erosion by ELMs' between CO + PERP NB and CTR + PERP NB injected H-mode discharges (Ip=1.6MA. Bt=3.95T, δ=0.36, κ=1.46, q_{95}=4.3). For CO+PERP, P_{inj}=9.3MW with 4.1MW of CO-tangential and 0.8MW of CTR-tangential NBs. For CTR+PERP, P_{inj}=10.5MW with 4.0MW of CTR-tangential NBs. (a) & (b): evolution of the stored energy (Wdia), Ti and Vt at various locations, and divertor D_α emission.

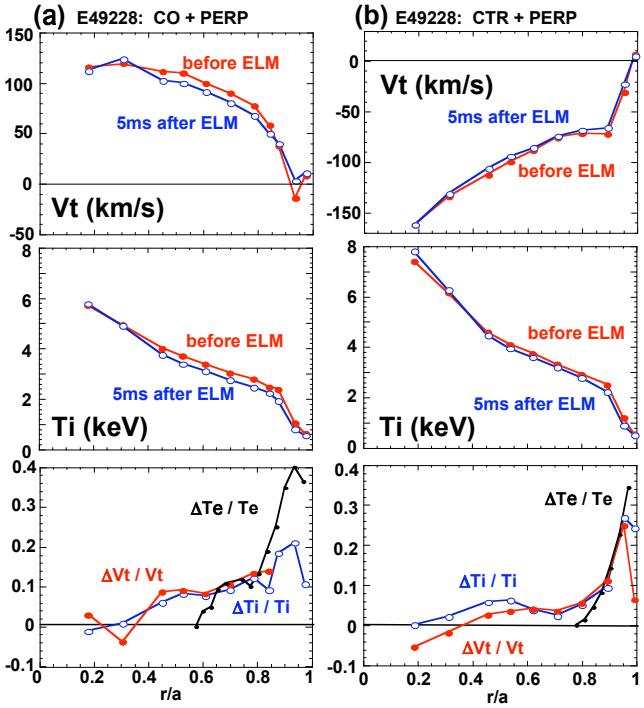

Fig.8 Change in T_i and V_t profiles across an ELM crash (just before the type I ELM crash and 5ms after the crash averaged for 3 ELMs (CO+PERP) and 5 ELMs (CTR+PERP)), and $\Delta V_t/V_t$, $\Delta T_i/T_i$ and $\Delta T_e/T_e$ for (a) CO-injection and (b) CTR injection cases shown in Fig.7

instability. However, the change within 5ms is much faster than the typical radial propagation time of momentum transport (which is a few 10 ms from r/a=0.8 to r/a=0.3 [12].

6. Change in rotation and temperature profiles by L-H Transition

Another key phenomenon affecting the ETB-ITB correlation is the L-H transition. JT-60 reported a sudden (within ms) edge-core connection appearing as change in the electron diffusion coefficient at ITB across L-H and H-L transitions [13]. Based on this knowledge, we have proceeded to investigation of the ion system. Here we treat BALANCE NB injected ITB cases in order to focus on the effects of intrinsic / spontaneous rotation effects. In case of CO or CTR torque input, change in momentum confinement at the ETB makes the interpretation more complicated.

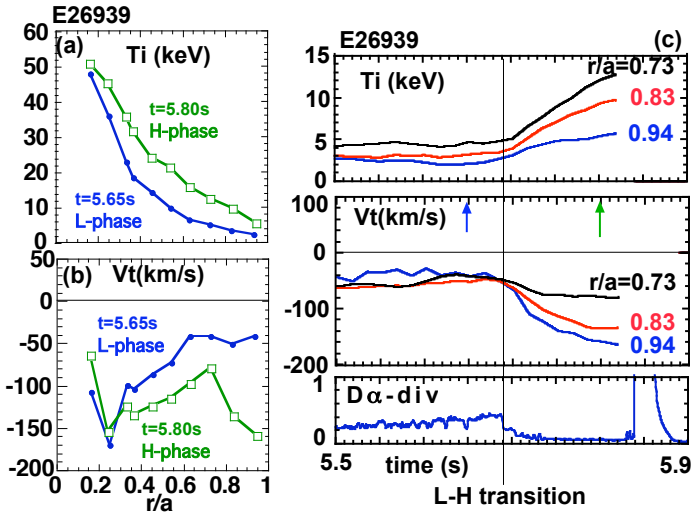

Fig.9: (a) & (b) change in T_i and V_t profiles across H-L transition and (c) evolution of the edge Ti, Vt and divertor D_α emission for a near-BALANCE injection Type I ELMing high β_p H-mode discharge (I_p=2.4MA, Bt=4.32T, δ=0.08, κ=1.74, q_{95}=2.93, P_{inj}=32.7MW with 4.5MW of CO-tangential and 5.2MW of CTR-tangential NBs).

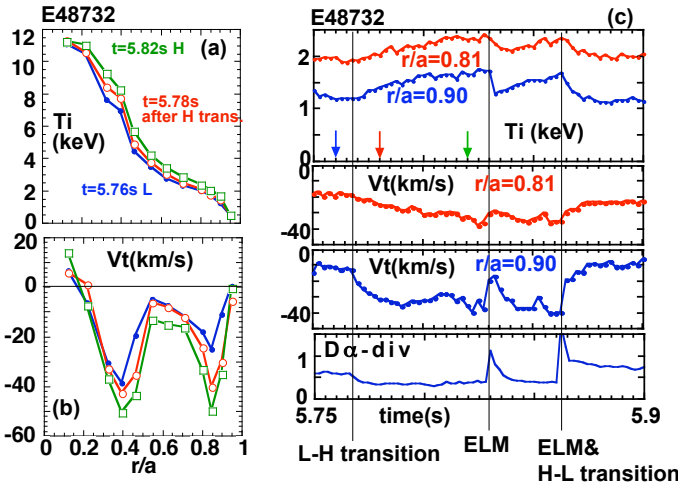

Fig.10: (a) & (b) change in T_i and V_t profiles across H-L transition, ELM, and ELM induced H-L back transition and (c) evolution of the edge Ti, Vt and divertor D_α emission for a BALANCE injection Type I ELMing high β_p H-mode discharge (I_p=1.0MA, Bt=3.04T, δ=0.19, κ=1.49, q_{95}=5.41, P_{inj}=11.3MW with 3.8MW of CO-tangential and 3.8MW of CTR-tangential NBs).

Figure 9 shows a high β_p H-mode at high plasma current at 2.4MA. The L-H transition occurs at t=5.68s, and Vt at r/a=0.94 shifts to the CTR direction promptly, then V_t in the inner region gradually moves to CTR direction with the time scale similar to T_i. In the L-mode phase (t=5.65s), the ITB structure in the T_i profile is clearly identified. On the other hand, in the H-phase, t=5.80s, smoothly peaked Ti profile is produced. By looking at the V_t profile, the region with a large CTR directed intrinsic rotation expands to r/a=0.75, and connected to the pedestal region having more largely CTR directed V_t.

Figure 10 shows a low I_p (1.0MA) case. The L-H transition occurs at t=5.767s, one type I

ELM occurs at t=5.83s, and ELM induced H-L back transition occurs at t=5.862s. After the L-H transition, similar to Fig.9, the edge V_t at r/a=0.90 shifts to the CTR direction promptly, then V_t in the inner region gradually moves to CTR direction with the time scale similar to T_i. In this case, the ITB structure is not so much affected by the H-transition, and the double-notch profile of Vt(r) with small V_t and V_t-shear at 0.5<r/a<0.7is kept in the H-phase.

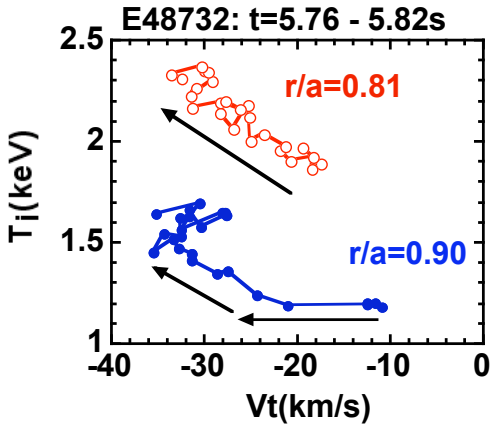

Fig.11: Evolution the edge Ti and Vt from just after the L-H transition to just prior to the ELM crash (t=5.76s - 5.82s) for the discharge shown in Fig.9 (BALANCE injection at Ip=1.0MA).

The relation of the edge V_t and T_i after the L-H transition is shown in Fig.11 for r/a=0.90 and r/a=0.81 for the same discharge shown in Fig.10. At r/a=0.9, V_t suddenly shifts to the CTR direction while T_i is constant, then V_t moves more CTR with increase in T_i at that location. In the inner region, r/a=0.80, the initial sudden change in V_t does not appear, and V_t and T_i moves with the same time scale. This initial spin up is similar to that reported by DIIID [14]. Also, just after the ELM crash, t=5.83s in Fig.10, the recovery of the edge CTR rotation is much faster than Ti. At the H-L back transition, t=862s in Fig.10, the edge CTR rotation is promptly lost. This edge Vt dynamics is almost the same as reported in Ref.[15].

As shown in Figs.9 and 10, the total V_t profile over the ITB and ETB regions are largely affected by the L-H transition. It should be noted again that the evolution of the V_t profiles shown in Figs.9 -11 are observation of BALANCED injection where intrinsic rotation by pressure gradient and spontaneous edge CTR rotation by H-mode.

7. Summary

For understanding of the physics processes determining the radial profiles of the plasma pressure in the advanced tokamak plasmas, correlation between ETB and ITB has been studied. We fond that $\beta_{p\text{-}ped}$ increases almost linearly with the total β_p over a wide range of the plasma current for the type I ELMing H-mode, and the dependence becomes stronger with increasing triangularity. This dependence is not due to the profile stiffness. With increasing the stored energy inside ITB (W_{ITB}), the total thermal stored energy (W_{th}) increases and then the pedestal stored energy (W_{ped}) increases. With increasing W_{ped}, the ELM penetration depth expands more inward and finally reaches the ITB-foot radius. At this situation, the ITB radius cannot move outward and the ITB strength becomes weak. Then the fractions of W_{ITB} and W_{ped} to W_{th} become almost constant. We also found that the type I ELM expels/decreases edge toroidal momentum larger than ion thermal energy. The ELM penetration radius for toroidal rotation tends to be deeper than that for ion temperature, and can exceeds the ITB radius. The ELM affected area is deeper for CO rotating plasmas than CTR rotating ones. The ELM affected area is deeper in the order of V_t, T_i and then T_e. The L-H transition also changes the V_t-profile more significantly than the T_i-profile. After the L-H transition, in the

ELM-free phase, the pedestal V_t sifts into the CTR direction deeply and suddenly, and after that the pedestal V_t and T_i evolves in the similar timescale. The change in V_t by ELM and L-H transition may affect degradation / evolution of ITBs.

Acknowledgements
This work was partly supported by JSPS 19560834. The authors thank Prof. P. Diamond, Dr. A.Leonard, Dr. C. Maggi for critical discussions in conducting this study.

References:

[1] ' ITER Phys. Basis', Nucl. Fusion 39 (1999) 2137.
[2] 'Progress in the ITER Physics Basis', Nucl. Fusion 47 (2007) S1.
In particular, E.J.Doyle, W.A.Houlberg, Y. Kamada et al., 'Chaper 2. Plasma Confinement and Transport' Nucl. Fusion 47 (2007) S18.
[3] Y.Kamada, H.Takenaga, A.Isayama, et al., Plasma Phys. Control. Fusion **44** (2002) A279.
[4] Y.Kamada, N.Oyama, S. Ide, et al., Plasma Phys. Control. Fusion **48** (2006) A419.
[5] C.F. Maggi, R.J.Groebner, N. Oyama, et al., *Nucl. Fusion* **47** No 7 (July 2007) 535
[6] H.Shirai, M. Kikuchi, T. Takizuka et al., Nucl. Fusion **39** (1999) 1713.
[7] Y.Sakamoto, T. Suzuki, S. Ide et al., Nucl. Fusion **44** (2004) 876.
[8] M. Yoshida, Y. Koide, H. Takenaga et al., Plasma Phys. Control. Fusion **48** (2006) 1673.
[9] M. Yoshida, Y. Kamada, H.Takenaga et al., Phys. Rev. Lett. **100** (2008) 105002.
[10] N.Oyama, Y. Sakamoto, A. Isayama et al., Nucl. Fusion **45** (2005) 871.
[11] H. Urano, N. Oyama, K. Kamiya et al., Nucl. Fusion **47** (2007) 706
[12] M.Yoshida, Y.Kamada, H.Takenaga, et al., Plasma and Fusion Research **3** (2008) S1007.
[13] S.V.Neudatchin, T.Takizuka, H.Shirai, et al., Plasma Phys. Cont. Fusion **44** (2002) A383
[14] M. R. Wade, K. H. Burrell, J. T. Hogan, et al., Phys. of Plasmas 12, (2005) 056120.
[15] M.Yoshida, S.Kobayashi, H.Urano, Plasma Phys. Cont. Fusion **48** (2006) A209